Superposed epoch analysis of MagnetosphericConvection Electric Fieldduring geomagnetic storms due to High SpeedSolar Wind during solar cycle 24

Abstract

The present study concerns the time variation of the MCEF with respect to geomagnetic phases as shown by SymH time variation by means of a superposed epoch analysis during solar cycle 24 for HSSW.For this work the magnetosphere input energy behavior is also highlighted. During IP and MP, the main effect of storm is the drop of MCEF and the decreasing particles density especially during the storm MP. During MP and RP, there is convection into a magnetosphere and the time for the total releasing of magnetosphere energy is longer that devoted to the RP. From IP to MP + RP, are pointed out the substorm onsets and the presence of substorms during the MP. From IP to MP + RP, the substorms that occur during the MP and the generated storms are not HILDCAA.

Keywords

Superposed epoch analysis, Magnetospheric convection electric fields, solar wind high speed, geomagnetic storm, geomagnetic indices

Introduction

Geomagnetic storm can be defined as a major disturbance of Earth's magnetosphere due to an efficient exchange of energy from the solar wind into the space environment surrounding Earth. The primarily causes of geomagnetic storms at Solar are Coronal Mass Ejections (CMEs) and High-Speed Solar Wind streams (HSSW). According to Gonzalez (1994) the primarilysources of geomagnetic storms at Earthare strong dawn-to-dusk electric fields associated withthe passage of southward directed Interplanetary MagneticFields (IMF), B_z, past the Earth for sufficiently long intervalsof time.

When CMEs and/or HSSW interact with Earth's magnetic field, they can provoke significantchanges in the magnetosphere with various effects on Earth (McPherron et al., 2008). During this disturbance,(MCEF plays a key role. Many studies (e.g. Akhavan-Tafti et al., 2023; Alqeeq et al., 2025; Kim et al., 2025; Bazie et al., 2025 and Desta et al., 2026)are performed to study magnetosphere variability during geomagnetic storms.Storms caused by CMEs have been particularly well-studied(e.g. Gopalswamy N., 2002; Pulkkinen et al., 2007; Gopalswamy N., 2009; Benacquista et al., 2010; Ontiveros et al., 2010; Liou et al., 2016; Kabore et al., 2018; Pedersen et al., 2022 and Bazie et al. 2025)but those due to high-speed solar winds are less.Several scientists (e.g. Denton et al., 2006, Borovsky et al., 2006),Hutchinson et al., 2011) andGrandin et al., 2019)showed that HSSW storms are different from CMEs storms. It is therefore important to carry out analyses specific to these storms. The present study focuses on 20 storms caused by high-speed winds and/or CIRs during the declining phase of solar cycle 24. In this study, we attempt to answer the following questions: How does the convective electric field vary during the different phases of storms caused by high-speed solar winds? What are the solar wind parameters that determine the state of the magnetosphere during each phase of a storm caused by high-speed solar winds? To answer these questions, we use a statistical storm-phase approach. Several studies have shown that the phase-based approach is useful for understanding the processes involved during magnetic storms (Wang et al. 2024; Mishra et al. 2024; Ahmed et al. 2024). However, the study of storms presents a major complexity: the events do not have the same durations, and the phases of the storm do not have the same characteristics. In order to standardize them and extract average trends for each phase, we use a superposed epoch analysis with time normalization.It is important to note that this method has been used to study geomagnetic storms by Hutchinson et al. (2011) for the intensity of the storms.; Yermolaev et al. (2010) for the average behavior of the geomagnetic storms; Keesee et al. (2014) for studying the global ion temperature during the ICME driven and CIR driven storms; Katsavrias et al.(2019) for the acceleration and loss of relativistic electron. To improve the accurate behavior of the storm Yokoyama and Kamide (1997) and Manu et al. (2023) used Double superposed epoch analysis.

For us, the superposed epoch analysis allows on one hand, to equalize storms over the same normalized time intervals, and also to deduce the mean, median, as well as the lower and upper quartiles of the different parameters for each normalized time. These values allow us to compare the variation of the magnetospheric convection electric field across the three phases

and to extract the average variation during storms in order to answer the first question. To answer the second question, we analyze the relationship between solar wind parameters and the MCEF throughout the different phases of storms. In the following, we will describe the data and the methods and we will present the results.

1. Data and methodology

1.1 Data

Magnetospheric activities, geomagnetic storms, substorms are due to the energy injected into the magnetosphere from the solar wind (Akasofu,1981). This energy injected is responsible for the dynamics of the magnetosphere-ionosphere system (Newell et al., 2007).To determine the energy input, several energy coupling functionsare used (Perreault and Akasofu, 1978; Kan and Lee, 1979; Murayama, 1982;Vasyliunas et al. 1982; Wygant et al. 1983; Bargatze et al., 1986; Xu and Shi, 1986; Mac-Mahon and Gonzalez,1997; Stamper et al., 1999; Koskinen and Tanskanen, 2002; Vichare et al., 2005; Finch and Lockwood, 2007; Wang et al., 2014). In this work the coupling function of Wang et al. (2014) is used.

The energy input can be predicted by means ofB_z component of the IMF, the solar wind velocity (V) and the dynamic pressure (p) (Dungey, 1961; Kan and Lee, 1979; Wygant et al., 1983; Scurry and Russell, 1991; Temerin and Li, 2006; Newell et al., 2007). It can be also noted that the magnetospheric state variables can be determined by using B_z.

Therefore, in the present study, the following data are used: solar wind velocity (V); the Z component of Interplanetary magnetic Field (IM (B_z) and the Y component of Interplanetary Electric Field (IEF) (E_y), solar wind particles density (n).

To determine storm time phases, we utilized the geomagnetic index SymH (according to Iyemori (1990), SymH measures the activity of ring current with 1 minute as time resolution and is same as Dst with 1 hour as time resolution. To estimate the overall intensity of auroral currents the Auroral Electrojet (AE) is used in this work.

This study focuses on the variation of the magnetospheric convection electric field (MCEF) under the influence of High-Speed Solar Wind (HSSW). It is important to note that this influence can be interpreted in terms of, on the one hand, energy injected into the magnetosphere as a function of the characteristics ofsolar wind parameters and, on the other hand, geomagnetic storms intensity and time variation. Therefore,we will use the geomagnetic activity indices SymH and AE and solar wind parameters that are available on the

OMNIWEB website https://omniweb.gsfc.nasa.gov/form/omni_min.html and recorded in Table 1.

Table1: Geomagnetic index and solar wind parameters

Parameters (Unit)	Resolution	Description	Utilisation
V (Km/s)	5 min	Solar wind speed	For analyzing changes in solar wind speed
B_z (nT)	5 min	Component along the z-axis of the interplanetary magnetic field	For analyzing conditions favorable to reconnection
E_y (mV/m)	5 min	Component of the electric field along the y-axis of the interplanetary magnetic field	For calculating the MCEF
AE (nT)	5 min	AE index for monitoring auroral activity	For evaluating auroral activity
SymH (nT)	5 min	Index quantifying variations in the ring current	For dividing storms into different phases
n, particles density (particles/cm^3)	5 min	Densité des particules du vent solaire	

1.2 Methodology

1.2.1Study of geomagnetic storms

a) Determination of geomagnetic storms

In this study that covers the period from 2008 to 2018, we focus on geomagnetic storms. The start of a storm is identified by the condition $\mathrm{SymH} < -60\ nT$ and the end by the condition $\mathrm{SymH} > -20\ nT$. There were 125 storms during the period in question, regardless of their origin or source.

Several classifications of storms exist:

a) Classification according to Hutchinson et al. (2011) and Walach et al. (2019).

Low-intensity storms: $-150\ \mathrm{nT} < \mathrm{SymH}_{min} \leq -80\ \mathrm{nT}$

Moderate storms: $-300\ \mathrm{nT} < \mathrm{SymH}_{min} \leq -150\ \mathrm{nT}$

Intense or strong storms: $\mathrm{SymH}_{min} \leq -300$ nT where $\mathrm{SymH}_{\mathrm{min}}$ is the minimum value of SymH

b) Classification according to Li et al. (2010; 2012)

Moderatestorms: 100 <SymH ≤ 50 nT

Intense storms: 300 <SymH ≤ 100 nT

Superstorms: SymH≤ 300 nT

For our work, we adopt the following criteria by adapting the two previous classifications:

Low-intensity storms: - 100 nT<SymH_{min}≤- 60 nT

Moderate storms: - 150 nT<SymH_{min}≤ - 100 nT

Intense storms: - 300nT<SymH_{min} ≤ - 150 nT

Superstorms: SymH_{min} ≤ - 300 nT

Applying these criteria gives the following classification: 95 low-intensity storms, 25 moderate storms, and 5intense storms.

Taking into account the fact that weak storms are caused by High-Speed Solar Wind (HSSW) and Corotating Interaction Regions (CIRs)and given that this study only concerns the magnetospheric convection electric field (MCEF) during storms caused by HSSW, we will use the following condition to deal with storms: $-150\ \mathrm{nT} < \mathrm{SymH}_{min} \leq -60\ \mathrm{nT}$. This is expressed as: Low-intensity storms: - 100 nT<SymH_{min}≤- 60 nT and Moderate storms: -150nT<SymH_{min}≤ - 100 nT

Under this condition, we impose the presence of HSSW or CIRs at the time of the storm to ensure that the storm in progress is mainly due to HSSW or a combination of both (HSSW/CIR).

Finally, storms that are mainly due to HSSW/CIR are identified by cross-referencing the list of HSSW and CIRs compiled by Katsavrias et al. (2025) and Katsavrias (2025) and available at https://zenodo.org/ records/15225254 with that of Coronal Mass Ejections (CMEs) and Magnetic Clouds (MCs) provided by the Interplanetary Coronal Mass Ejections Catalog (ICMEs) by Regnault et al. (2020) and available at https://idoc.ias.u-psud.fr/sites/idoc/files/CME_catalog/html/ACE-ICMEs-list-dates-quality-nosheath-forweb.html . This ultimately gives us 14low-intensity storms and 2 moderate storms. These are highlighted in table 2.

b) Geomagnetic storm time phases

The storm time is divided into three phases with respect to SymH time variation (figure 1): (a) the Initial Phase (IP) with time interval (t_0-t_1); the Main Phase (MP) characterized by a time interval (t_1-t_2)and the Recovery Phase (RP) with time interval(t_2-t_3) (table 2)

Table2: Start and End phases of the retained geomagnetic storms

Number of storm	Start of IP	Start of MP or End of IP	Start of RP or End of MP	End of RP	$SymH_{min}$
1	03/09/2008 14:50	03/09/2008 23:15	04/09/2008 03:05	04/09/2008 11:00	-67
2	10/10/2008 03:05	11/10/2008 07:20	11/10/2008 11:30	14/10/2008 22:55	-64
3	21/07/2009 03:20	21/07/2009 22:25	22/07/2009 05:55	25/07/2009 11:35	-93
4	01/05/2010 12:30	02/05/2010 08:15	02/05/2010 20:30	05/05/2010 05:35	-75
5	04/02/2011 07:05	04/02/2011 16:55	04/02/2011 21:20	07/02/2011 02:15	-67
6	01/03/2011 07:40	01/03/2011 09:20	01/03/2011 14:25	03/03/2011 11:50	-71
7	31/05/2013 13:55	01/06/2013 01:35	01/06/2013 07:45	03/06/2013 01:10	-134
8	07/12/2013 15:20	07/12/2013 22:40	08/12/2013 08:30	09/12/2013 05:50	-72
9	03/07/2015 23:10	04/07/2015 15:55	05/07/2015 04:55	07/07/2015 20:05	-86
10	05/03/2016 13:05	06/03/2016 15:00	06/03/2016 21:20	09/03/2016 03:05	-120
11	23/10/2016 02:40	23/10/2016 05:50	25/10/2016 22:55	28/10/2016 17:45	-80
12	26/03/2017 19:55	27/03/2017 01:00	27/03/2017 16:10	29/03/2017 20:45	-86
13	26/09/2017 19:55	27/09/2017 05:30	28/09/2017 05:50	29/09/2017 07:35	-74
14	06/11/2017 12:25	07/11/2017 04:35	08/11/2017 04:05	10/11/2017 01:00	-89
15	20/11/2017 07:40	20/11/2017 17:20	21/11/2017 06:50	24/11/2017 12:25	-60
16	05/05/2018 04:05	05/05/2018 14:20	06/05/2018 02:30	08/05/2018 01:35	-66

Figure 1: SymH time variation with storm time phases

1.2.2 Superposed Epoch Analysis method

Studying storms presents difficulties due to their different characteristics. Indeed, they have different durations and intensities. This makes it difficult to calculate averages per phase for a set of storms and to perform a general analysis of trends for each phase. An alternative is to use the method called "superposed epoch analysis with time normalization". For more details about this method see Walton and Murphy (2022). Their method execution code can be foundat the following link https://github.com/samwalton7645/SEA_Code.

To analyze storm parameters (B_z, AE, E_m, W_{recon}, W_{others}, n, SymH) , each storm SymH is divided into three phases (see figure 1). For analyzing each storm phase effect on the parameters, we define four cases that can be named events. To apply the Superposed Epoch Analysis (SEA) method, firstly, the event time must be divided into two parts named in the method phases. The first one, from the beginning of the event (t_{begin}) to the event development called by Walton and Murphy (2022) epoch (t_{epoch}) and the second one from the epoch (t_{epoch}) to the end of the event (t_{end}); secondly, each part time interval is normalized in order to transform it to a standard interval $[0\ 1]$; thirdly, the standard interval is binned into a set of equally spaced bins; fourthly, for each part interval, a set of statistics (mean, median, etc.) is then determined for thedata residing in each bin.

a) Time normalization

The SEA code is run four times with respect to the two parts or code phases per event. We have:

- Run 1: Obtention of parameters time variation for IP and MP

$$Code\_Phase\ 1 = IP \text{ and } code\_Phase\ 2 = MP$$

This is done for having on one hand the effects of IP and the effects of MP, on the other hand. The time intervals are (t_0-t_1) and (t_1-t_2)

- Run 2: Obtention of parameters time variation for MP and RP

$$Code\_Phase\ 1 = MP \text{and} Code\_Phase\ 2 = RP$$

The SEA code program is run for having on one hand, the effects of MP and the effects of RP, on the other hand. The time intervals are (t_1-t_2) and (t_2-t_3)

- Run 3: Obtention of parameters time variation for IP + MP and RP

$$Code\_Phase\ 1\text{=IP + MPand}Code\_Phase\ 2\ = RP$$

The SEA code script is executed for having on one the hand, the global effects of IP and MP together and on the other hand, the effects of RP.The time intervals are (t_0-t_2) and (t_2-t_3)

- Run 4: Obtention of storm parameters time variation for IP and MP + RP

$$Code\_Phase\ 1 = \text{IP and} Code\_Phase\ 2\ = MP + RP$$

This is done for having on one hand, the effects of IP and on the other hand, the global effects of MP and RP together. The time intervals are (t_0-t_1) and (t_1-t_3).

To apply SEA method, we convert each storm phase intervals into a standard one [0 1]. The process is:having$\forall t \epsilon [t_i; t_j]$with$i = 0,1,2andj = 1,2,3$we define the normalized time as follows: $t_{norm} = \frac{t-t_i}{t_j-t_i}$. This leads to a normalized interval so that for a given timet_{norm} we have$t_{norm}\ \epsilon [0; 1]$

For each phase and for each instant t, we calculate the time elapsed between the start of the phase and instant t. That is, the time elapsed between $t_0$and $t$for any instant t of phase 1 or between t_1 and t for any instant t in phase 2 or for any instant t between t_2 and t for any instant t in phase 3. Each elapsed time value is converted to a value between 0 and 1 by dividing it by the total duration of the phase. Thus, 0 corresponds to the beginning of the phase and 1 to the end of the phase. This means that regardless of the duration of the storms, they can be aligned on an evolution scale.

b) *binning into a set of equally spaced bins*

Firstly, each codephase standard interval is binned. The number of bins is given in table 3. Secondly, the binned normalized time is obtained by starting to count bins at the epoch time. Thus, bin numbers before epoch time are negatives and that after epoch time are positive.

Table 3: Number of bins per code phase forgiven Run

Run number	Number of bins forCode_Phase1	Number of bins forCode_Phase2
1	40	120
2	80	100
3	40	100

4	40	40

1.2.3Determination of Magnetospheric Convection Electric Field (MCEF)

To determine the values of the magnetospheric convection electric field (MCEF), we will use the relationship proposed by Wu et al. (1981) and validated by Revah and Bauer (1983), which links the E_y component of the Interplanetary Electric Field (IEF) to $B_z$component of the Interplanetary Magnetic Field (IMF):$E_M = 0.13\ E_y + 0.09$ with$E_y = -VB_z$ where V is the solar wind speed.

1.2.4Determination of the input energy components

To determine the energy transferred during the coupling between the solar wind and the magnetosphere, we will use the relationship described by Wang et al. (2014):

$W_{in} = 3.78\ 10^7 n^{0.24} V^{1.47} B_T^{0.86} [sin^{2.70}(\theta/2) + 0.25]$where:

$\theta$is the shock incidence angle of the interplanetary magnetic field. It is defined as follows:

$$\begin{cases} \theta = \tan^{-1}\left(\frac{B_y}{B_z}\right) if B_z > 0 \\ \theta = \pi - \tan^{-1}\left(\frac{B_y}{B_z}\right) if B_z < 0 \end{cases}$$

$V$the solar wind speed, $B_T$the IMF magnitude expressed as: $B_T = \sqrt{{B_y}^2 + {B_z}^2}$, n_{sw} the solar wind particles density.

The equation that gives the input energy can be rewritten as:

$W_{in} = 3.78\ 10^7 n^{0.24} V^{1.47} B_T^{0.86} sin^{2.70}\left(\frac{\theta}{2}\right) + 3.78\ 10^7 n^{0.24} V^{1.47} B_T^{0.86} 0.25$.

It can be seen that we have the sum of two expressions which can be expressed as:

$W_{recon} = 3.78\ 10^7 n^{0.24} V^{1.47} B_T^{0.86} sin^{2.70}\left(\frac{\theta}{2}\right)$and $W_{others} = 3.78\ 10^7 n^{0.24} V^{1.47} B_T^{0.86} 0.25.$

therefore $W_{in} = W_{recon} + W_{others}$

The first term (W_{recon}) represents the injected electromagnetic energy, mainly due to magnetic reconnection on the day side, which varies with$\sin^{2.70}(\frac{\theta}{2})$. This term reaches its

maximum when the IMF is oriented towards the south ($\theta = 180\,°$ and $\sin\left(\frac{\theta}{2}\right) = 1$) and cancels out when the IMF is oriented towards the north ($\theta = 0°$).

The second term (W_{others}) represents an energy contribution independent of the clock angle, attributed to other processes such as reconnection at high latitudes (in the lobes), viscous interactions, or mechanical energy transfer (e.g., via Kelvin–Helmholtz instabilities). This component becomes relatively more important when the IMF is oriented northward.

2. ResultsandDiscussions

Figures 2-6 show the bin normalized time (BNT) for some solar wind parameters (particles density, Z component of IMF), the geomagnetic indices AE and SymH and the calculated injected energy from solar wind into the magnetosphere components (reconnexion energy and other sources of energy).

In figures 2-5, panel a concerns AE index, panel b is devoted to Bz, panel c shows the BNT evolution of SymH, panel d concerns particles density, panel e, presents the BNT variation of MCEF and panels f and g are devoted to W_{recons} and W_{others}, respectively.

2.1. Case of Run 1

In figure 2 BNT varies from - 40 to 39 BNT with IP (from - 40 to 0 BNT) and MP (from 0 to 39 BNT). It can be seen that during IP all parameters exhibit constant value close to zero, exceptparticles density and the injected energy due to other sources. This observation let us say before storm (1) there is no convection electric, (2) magnetosphere is submitted to input energy independently to the coupling solar wind magnetosphere interactions; (3) the particles density is remained at 12.5 particles /cm^3.When Bz decreases and tends toward zero there is a slight increase of other sources input energy and particles density. When Bz passes from northward to southward we enter into MP and we observe a sudden increase of all parameters. During the remain southward Bz, the particles density decreases and tends toward a value before the begining of the storm. For the other parameters, they slightly increase. At the end of MP, the reconnected input energy drops from 0 W to 3 W while that of the other sources passes from 0.25 W to 1.25 W and the MCEF value goes from 0 mV/m to 0.4 mV/m.

The main effect of storm is the drop of all parameters since Bz passes southward and the smooth increase of all parameters except the particles density which highlights a maximum when Bz passes southward and after decreases. This shows the loss of particles during storm MP.

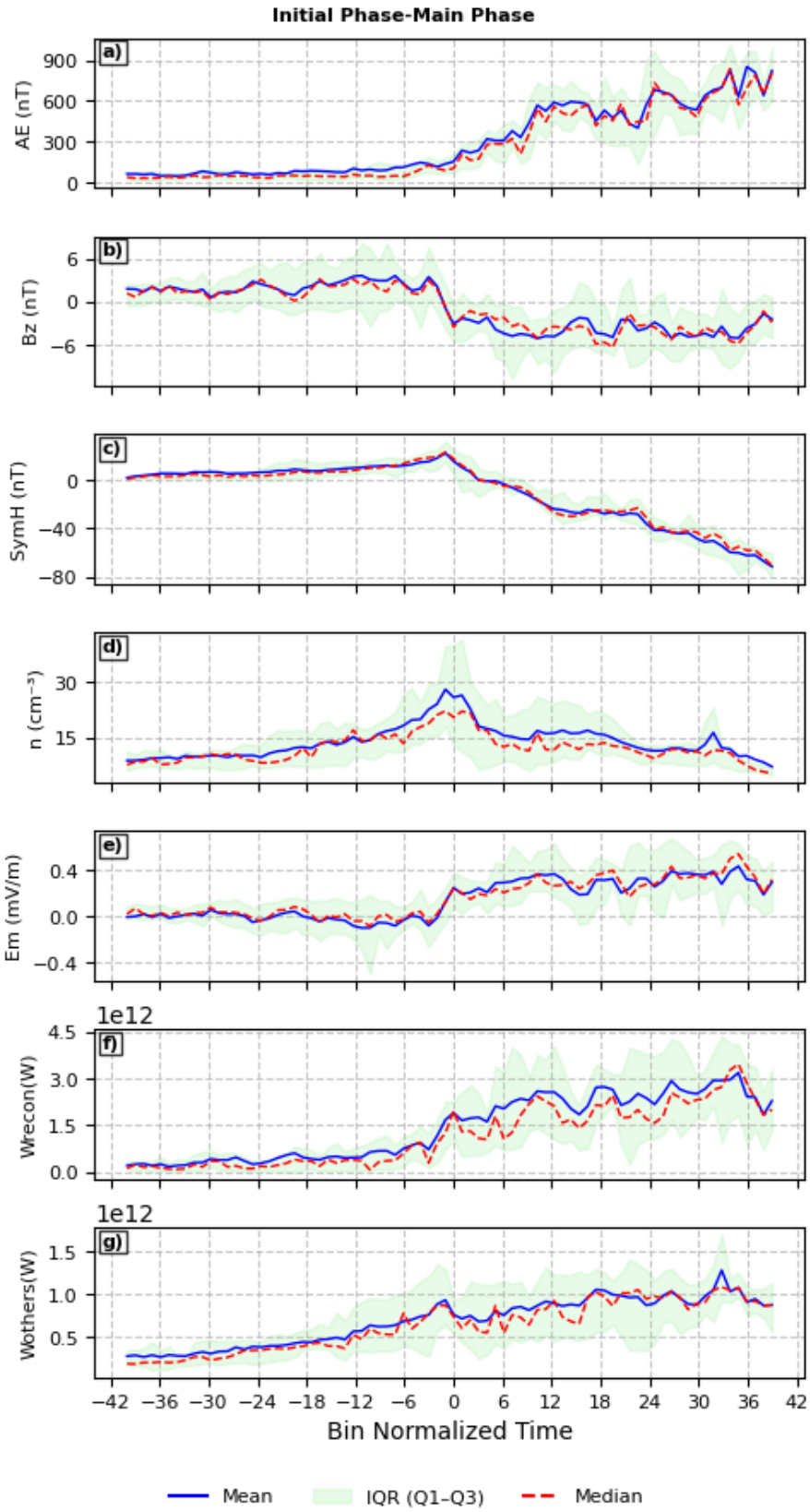

Figure 2: Solar wind parameters and geomagnetic indices BNT variation during IP and MP. From top to bottom: a) AE index; b)Bz; c)SymH; d) particles density; e) MCEF; f) input energy due to reconnection and g) input energy due to the other sources

2.2. Case of Run 2

Figure 3 shows BNT evolution of solar wind parameters and geomagnetic indices (SymH and AE) and input energy components for MP and RP. BNT varies from -40 to 0 for MP and from 0 to 100 for RP. It can be seen, when B_z remains southward, the decreasing of SymH and particles density and the increasing of the other parameters. At the minimum value of SymH (- 75 nT), the end of MP and the beginning of RP, B_z reaches 0 nT, AE its maximum value (850 nT). Particles density, MCEF, and input energy curves present a maximum (15 particles/cm^{-3}, 0.5 mV/m, 3 W and 1.3 W, respectively) before the end of MP at -5 BNT. During RP, all parameters decrease and tend smoothly toward 08 mV/m for MCEF, 0.5 W for the reconnecting energy and 0.25 W for that due to other sources.

The MCEF not reaches 0 mV/m that exhibits the remain of convection into the magnetosphere, even though there is a decreasing of the input energy, it is not totally dissipated after the end of storm. Thispointed out that there is remaining energy at the end of the storm. Consequently, the input energy is not completely dissipated. The consequence is that the time for total releasing of magnetosphere energy is longer that devoted to the RP.

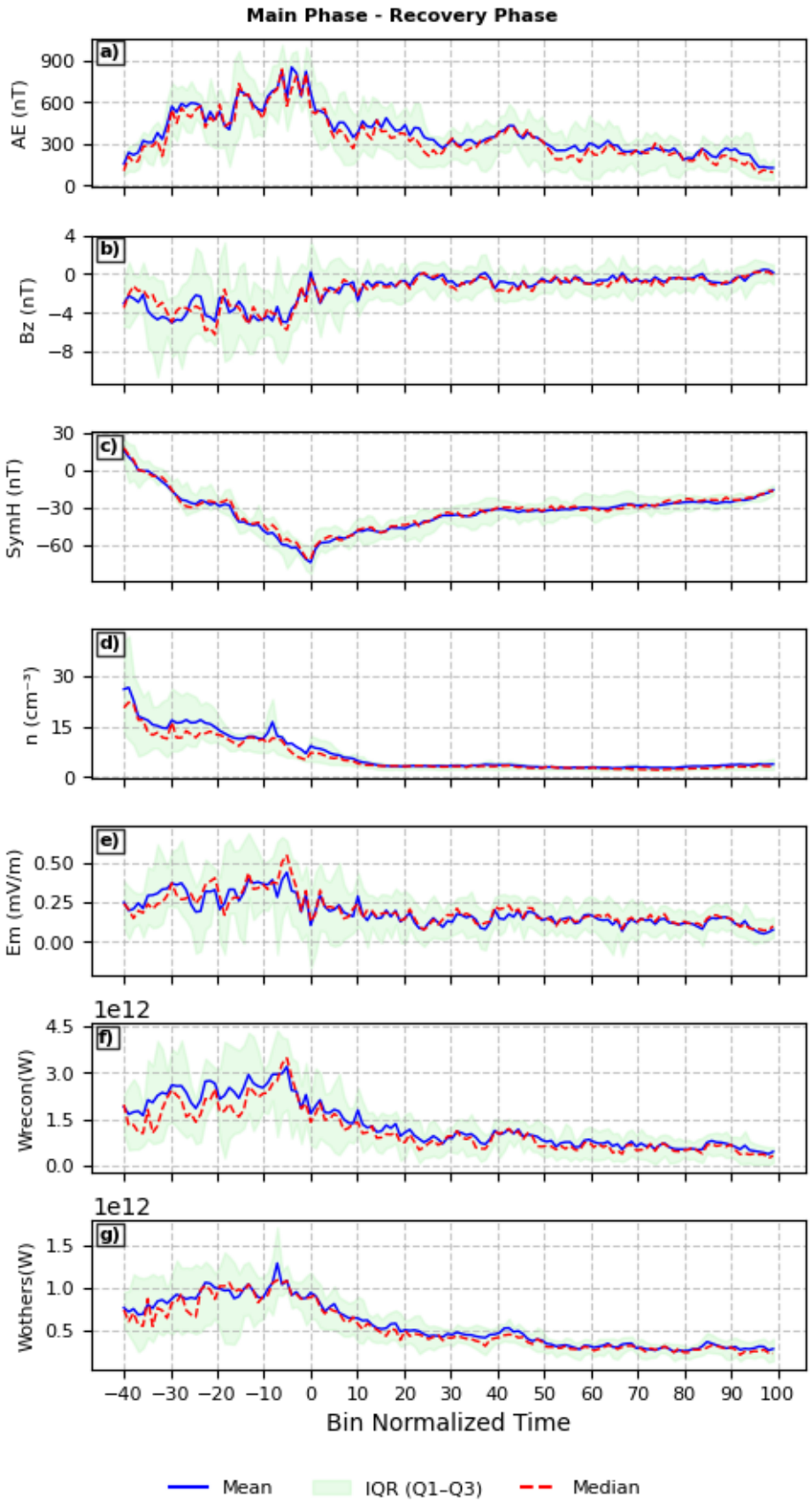

Figure 3: Same as Figure 2 but during MP and RP

2.3. Case of Run 3

Figure 3 presents two parts of storm time variation: the whole IP and MP (from -80 BNT to 0 BNT) as the first part and the RP (from 0 BNT to 99 BNT) as the second part.

During the whole IP and MP, the parameters (AE, n, E_m, W_{recon}, W_{others}) simultaneously increase and during RP they decrease at the same time and tend toward their minimum value.

At -40 BNT B_z becomes northward and parameters decrease. AE, MCEF and reconnection input Energy are more sensitive to this change in B_z direction. When B_z passes from northward to southward, AE increases until the end of MP and decreases after. Its minimum value is superior to that before storm. This proves that the magnetosphere does not return to its initial state after the storm has passed. The particles density decreases when $B_z$turns southward and stabilizes at 2 particles/cm^3close very lower than its value (8 particles/cm^3) before the storm. Everything happens as the storm depletes the magnetosphere from a particle perspective.

The MCEF increases when B_z passes southward and starts decreasing before the end of MP. The decrease continues during the recovery phase, tending towards zero and very close to the state before the storm. We can conclude that the magnetospheric convection electric field created by the storm fades away at the end of the storm.

The variability of input energy is the same as that of MCEF but with a pronounced slope at the beginning of the decreasing. The final value (0.38 W) at the end of the storm is higher than that before storm (~0 W) for the input energy due to reconnection while the input energy coming from the other sources last value (~039 W) is the same as before the storm. We can conclude that the magnetosphere gains energy after the storm in terms of energy due to reconnection despite tail reconnection and substorm activity allow the system to return to a more normal configuration with respect to the size of the storm (Hutchinson et al., 2011; Gonzalez et al., 1994; Daglis et al., 1999; Liemohn et al., 1999 and Reeves et al., 2003)

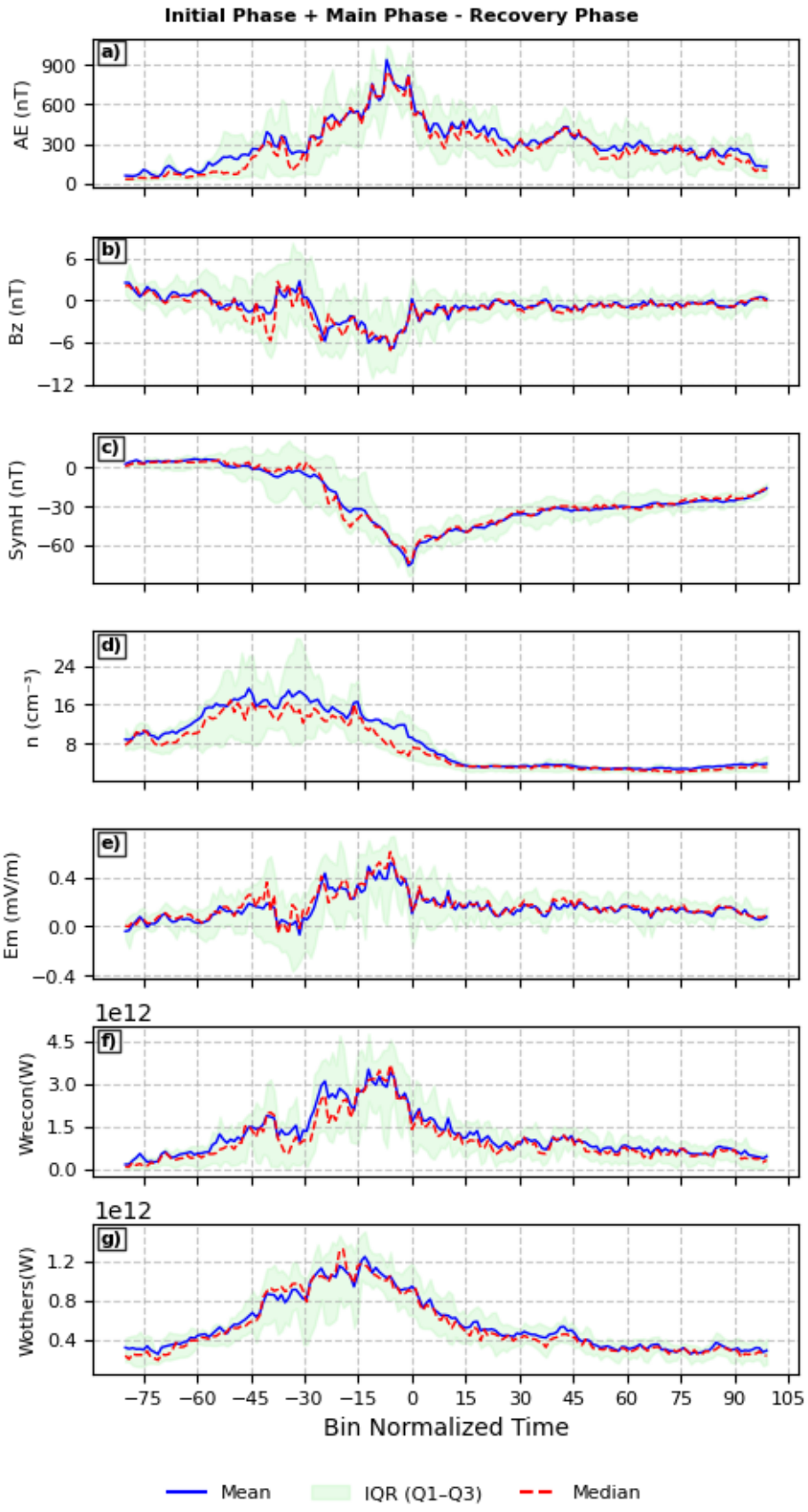

Figure 4: Same as Figure 2 but during IP +MP and RP

2.4. Case of Run 4

Figure 4 shows the evolution through all storm phases in accordance with the temporal evolution of SymH of the parameters AE index, IMF component B_z, the density of particles in the magnetosphere n, the MCEF Em, and the components of energy injected into the magnetosphere, namely the reconnection component W_{recon} and the component due to other sources W_{others}. In this figure, the IP starts from -42 bin normalized time (BNT). and ends at 0 BNT. The whole main and recovery phases (MP and RP) start from 0 to 120 BNT. At 0 BNT, the IMFB_z turns from northward to southward and reaches its minimum at 7.5 BNT. At the same time (0 BNT) all parameters increase and reach their maximum at 7.5 BNT.

We have 610 nT, for AE; - 10 nT for B_z;40.6 mV/m for Em, 3.75 W for W_{recon} and 1 W for W_{others}. The particles density n reaches its maximum at 0 BNT with 30 cm^{-3}. During the RP, the MCEF decreases and fluctuates around a level slightly higher than the level before the storm

The particles density decreases and reaches a level lower than that before the storm. The injected energies (W_{recon} and W_{others}) and AE index decrease and stabilize at levels slightly higher than those before the storm.

The prompt increases of AE at 0 BNT when B_z turns from northward to southward lets us assert that at this time there is an increase of the overall intensity of auroral current (Nakamura et al., 2015) and characterizes not only a substorm onsets (Wang et al., 2014) but also the presence of substorms because these are observed to occur during the MP of magnetic storms (Gonzalez, 1994). As the sudden increases of AE index appears during the MP instead of RP and AE values are less than 1000 nT it emerges that the present storm events are not those qualified by Tsurutani and Gonzalez (1987) and Hajra et al. (2014) High-Intensity, Long-Duration, Continuous AE Activity (HILDCAA) events.

The maximum AE reached during the main phase and its subsequent exponential decrease confirms the assumption made by Kamide and Fukushima (1971) that the rate of energy injection into the annular current depends on the AE index.

Figure 4 exhibits that solar wind velocity increases when the particles density decreases. This expresses the behavior of storms provoked by CIRs as asserted by Hutchinson et al. (2011).

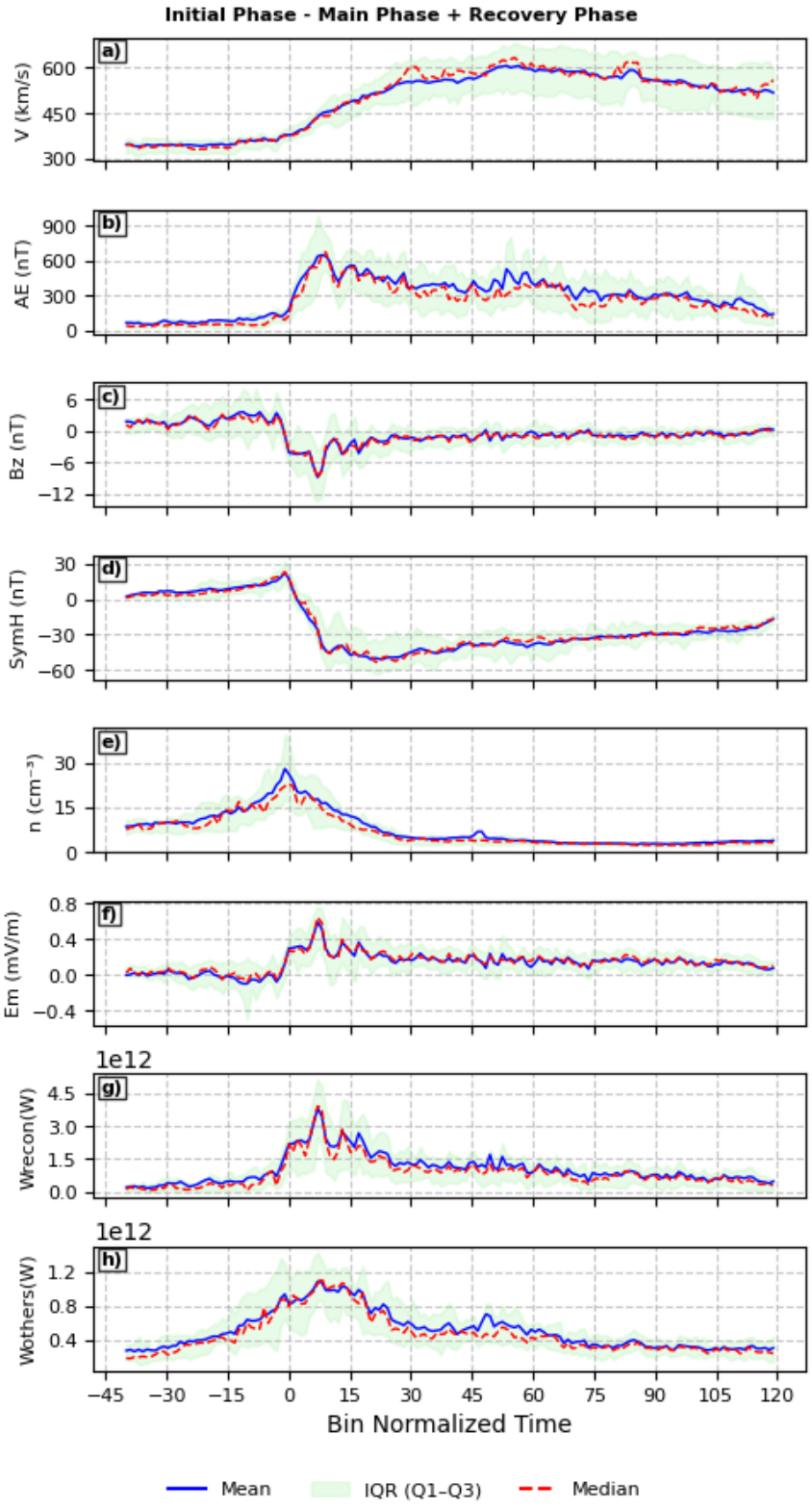

Figure 2: Solar wind parameters and geomagnetic indices BNT variation during IP and MP +RP. From top to bottom: a) Solar wind velocity; b)AE index; c); Bz; d) SymH; e)

particles density; f) MCEF; g) input energy due to reconnection and h) input energy due to the other sources

Conclusion

The MCEF time variation was studied by means of superposed epoch analysis during geomagnetic storms caused by HSSW for solar cycle 24. The analysis of MCEF through the three phases of storm time with respect to SymH variation shows that: From IP to MP, the main effect of storm is the drop of MCEF since B_z passes southward and its smooth increasing during the storm MP. From the MP to RP, the convection remains into the magnetosphere even though there is a decreasing of the input energy. This energy does not completely dissipate. From IP + MP to RP the MCEF created by the storm fades away at the end of the storm. The magnetosphere gains energy after the storm in terms of energy due to reconnection despite tail reconnection and substorm activity allow the system to return to a more normal configuration.From IP to MP + RP, we have the substorm onsets during the storm MP and the behavior of storms due to CIRs. The concerning storms are different to those of HILDCAA events.

Bibliography

Ahmed O., B. Badruddin, and M. Derouich. "Characteristics and development of the main phase disturbance in geomagnetic storms (Dst⩽-50nT)." Advances in Space Research 73.9 , 4453-4481, 2024

Akhavan-Tafti M., Atilaw T. Y., Fontaine D., Le Contel O., Slavin J. A., & Pulkkinen T,. Magnetospheric time history in storm-time magnetic flux dynamics. Journal of Geophysical Research: Space Physics, 128, e2023JA031832, 2023 https://doi.org/10.1029/2023JA031832

Alqeeq S., Fontaine D., Le Contel O., Akhavan-Tafti M., Cazzola E., &AtilawT. , Quantitative estimates of the magnetic flux variations in the inner magnetosphere during an intense storm. In EGU General Assembly Conference Abstracts , pp. EGU25-8724, 2025.

Bargatze L. F., R. L. McPherron, and D. N. Baker. Solar wind-magnetosphere energy input functions, in Solar Wind-Magnetosphere Coupling, edited by Y. Kamide and J. A. Slavin, pp. 93–100, Terrapub/Reidel, Tokyo, Japan, 1986

Bazié N., S. Kaboré, K. Guibula, F. Ouattara, Response of the Magnetospheric Convection Electric Field (MCEF) to Geomagnetic Storms During the Solar Cycle 24 Maximum Phase, International Journal of Geophysics, 2025, 9888419, 19 pages, 2025. https://doi.org/10.1155/ijge/9888419

Benacquista R., S. Rochel, G. Rolland , Understanding the variability of magnetic storms caused by ICMEs. In : Annales Geophysicae. Göttingen, Germany : Copernicus Publications,. p. 147-159, 2017

Borovsky J. E., and M. H. Denton , Differences between CME-driven storms and CIR-driven storms, J. Geophys.Res., 111, A07S08, 2006 doi:10.1029/2005JA011447

Daglis I. A., R. M. Thorne, W. Baumjohann, and S. Orsini. The terrestrial ring current: Origin, formation, and decay, Rev. Geophys., 37(4),407–438, 1999. doi:10.1029/1999RG900009.

Denton M. H., J. E. Borovsky, R. M. Skoug, M. F. Thomsen, B. Lavraud, M. G. Henderson, R. L. McPherron, J. C. Zhang, and M. W. Liemohn , Geomagnetic storms driven by ICME- and CIR-dominated solar wind, J. Geophys. Res., 111, A07S07, 2006 doi:10.1029/2005JA011436

Desta E. T., S. Kumar, M.B. Moldwin, M.-C. Fok, EA Kebede, TH Eritro, Solar wind-driven magnetospheric current variability during 2013 storms: Ground and space observations, Advances in Space Research,Volume 77, Issue 1 , Pages 1138-1156, 2026 https://doi.org/10.1016/j.asr.2025.11.098.

Dungey J. W. Interplanetary magnetic field and auroral zones, Phys. Rev. Lett., 6, 47, 1961

Finch I., and M. Lockwood. Solar wind-magnetosphere coupling functions on timescales of 1 day to 1 year, Ann. Geophys., 25(2), 495–506, 2007

Gonzalez W. D., J. A. Joselyn, Y. Kamide, H. W. Kroehl, G. Rostoker, B.T. Tsurutani, and V. M. Vasyliunas, What is a geomagneticstorm?, J. Geophys. Res., 99(A4), 5771–5792, 1994. doi:10.1029/93JA02867

Gopalswamy Nat. The CME link to geomagnetic storms. Proceedings of the International Astronomical Union, vol. 5, no S264, p. 326-335, 2009.

Gopalswamy N. Relation between coronal mass ejections and their interplanetary counterparts. In : COSPAR Colloquia Series. Pergamon,. p. 157-164, 2002

Grandin M., Aikio A. T., & Kozlovsky A. Properties and geoeffectiveness of solar wind high-speed streams and stream interaction regions during solar cycles 23 and 24. Journal of Geophysical Research: Space Physics, 124, 3871–3892 ,2019 . https://doi.org/10.1029/2018JA026396

Hajra R., E. Echer, B. T. Tsurutani, and W. D. Gonzalez, Solar wind magnetosphere energy coupling efficiency and partitioning: HILDCAAs and preceding CIR storms during solar cycle 23, J. Geophys. Res. Space Physics, 119, 2675–2690, 2014 doi:10.1002/2013JA019646

Hutchinson J. A., D. M. Wright, and S. E. Milan Geomagnetic storms over the last solar cycle: A superposed epoch analysis J. Geophys. Res. vol. 116, A09211, 2011. doi:10.1029/2011JA016463

Iyemori T. Storm-time magnetospheric currents inferred from mid-latitude geomagnetic field variations, J. Geomagn. Geoelectr., 42, 1249–1265, 1990

Kamide Y., and N. Fukushima, Positive geomagnetic bays in evening high-latitudes and their possible connection with partial ring current, Rep. Ionos. Space Res. Jpn., 25, 125, 1971.

Kan J. R., and L. C. Lee. Energy coupling and the solar wind dynamo, Geophys. Res. Lett., 6, 577, 1979.

Katsavrias C., Daglis I. A., & Li W. On the statistics of acceleration and loss of relativistic electrons in the outer radiation belt: A superposed epoch analysis. Journal of Geophysical Research: Space Physics, 124,2755–2768, 2019. https://doi.org/10.1029/2019JA026569

Katsavrias C. « SIR/HSS List from Wind (1995 - 2022) ». Zenodo, 15 avril 2025. https://doi.org/10.5281/zenodo.15225254.

Katsavrias C., S. Di Matteo, L. Kepko, N. M. Viall, The dependence of periodic density structures' amplitude and length scale on solar wind density within stream interaction regions ,Astronomy&Astrophysique, 696 ,L20, 2025, https://doi.org/10.1051/0004-6361/202554483

Keesee A., M. Elfritz, J. G., Fok, M. C., McComas, D. J., & Scime, E. E. Superposed epoch analyses of ion temperatures during CME- and CIR/HSS-driven storms. Journal of Atmospheric and Solar-Terrestrial Physics, 115(116), 67–78, 2014. https://doi.org/10.1016/j.jastp.2013.08.009

Kim K.-H., Lee J., & Kistler L., Temporal and spatial evolution of cold ions in the inner magnetosphere during large magnetic storms. Geophysical Research Letters, 52, e2025GL115846, 2025 https://doi.org/10.1029/2025GL115846

Koskinen, H. E. J., and E. Tanskanen, Magnetospheric energy budget and the epsilon parameter, J. Geophys. Res., 107(A11), 1415, 2002. doi:10.1029/2002JA009283

Li H., C. Wang, and J. R. Kan, Midday magnetopause shifts earthward of geosynchronous orbit during geomagnetic superstorms with Dst ≤ 300 nT, J. Geophys. Res., 115, A08230, 2010. doi:10.1029/2009JA014612.

Li H., C. Wang, W. Y. Xu, and J. R. Kan. Characteristics of magnetospheric energetics during geomagnetic storms. Journal of Geophysical Research, Vol. 117, A04225, 2012. doi:10.1029/2012JA017584.

Liemohn M. W., J. U. Kozyra, V. K. Jordanova, G. V. Khazanov, M. F. Thomsen, and T. E. Cayton. Analysis of early phase ring current recovery mechanisms during geomagnetic storms, Geophys. Res. Lett., 26(18), 2845–2848, 1999 doi:10.1029/1999GL900611.

Mac-Mahon R. M., and W. D. Gonzalez, Energetics during the main phase of geomagnetic superstorms, J. Geophys. Res., 102, 14,199–14,207, 1997.

Manu V., Balan N., Zhang Q.-H., and Xing Z.-Y. Double superposed epoch analysis of geomagnetic storms and corresponding solar wind and IMF in solar cycles 23 and 24. Space Weather, 21, e2022SW003314, 2023. https://doi.org/10.1029/2022SW003314

McPherron R. L., J. M. Weygand, Tung-Shin Hsu, Response of the Earth's magnetosphere to changes in the solar wind, Journal of Atmospheric and Solar-Terrestrial Physics, 70, Issues 2–4, Pages 303-315, 2008 https://doi.org/10.1016/j.jastp.2007.08.040.

Mishra W., P. S. Sahani, S. Khuntia, D. Chakrabarty, Distribution and recovery phase of geomagnetic storms during solar cycles 23 and 24, Monthly Notices of the Royal Astronomical Society, Volume 530, Issue 3, , Pages 3171-3182, 2024 https://doi.org/10.1093/mnras/stae1045

Moraes-Santos S. P., Cândido C. M. N. , Becker-Guedes F. , Nava B., Klausner V., Borries C. , F. S. Chingarandi & Osanyin T. O. . Influence of Solar wind high-speed streams on the Brazilian low-latitude ionosphere during the descending phase of solar cycle 24. Space Weather, 22(12), 2024 e2024SW003873.

Murayama T. ,Coupling function between solar-wind parameters and geomagnetic indexes, Rev. Geophys., 20(3), 623–629, 1982 doi:10.1029/RG020i003p00623.

Nakamura M. , A. Yoneda, M. Oda and K. Tsubouchi, Statistical analysis of extreme auroral electrojet indices, Earth, Planets and Space 67:153 , 2015 DOI 10.1186/s40623-015-0321-0

Newell P. T., T. Sotirelis, K. Liou, C.-I. Meng, and F. J. Rich. A nearly universal solar wind-magnetosphere coupling function inferred from 10 magnetospheric state variables, Journal of Geophysical Research, vol. 112, A01206, doi:10.1029/2006JA012015, 2007

Ontiveros V., and J. Americo Gonzalez-Esparza. "Geomagnetic storms caused by shocks and ICMEs." Journal of Geophysical Research: Space Physics 115.A10 (2010).

Pedersen M. N., Vanhamäki H., Aikio A. T., Waters C. L., Gjerloev J. W., Käki S., &Workayehu A. B. , Effect of ICME-driven storms on field-aligned and ionospheric currents from AMPERE and SuperMAG. Journal of Geophysical Research: Space Physics, 127(8), 2022 e2022JA030423.

Perreault P., and S. I. Akasofu (1978), A study of geomagnetic storms, Geophys. J. R. Astron. Soc., 54, 547–573, 1978

Pulkkinen T. I., Partamies N., Huttunen K. E. J., Reeves G. D., & Koskinen H. E. J. Differences in geomagnetic storms driven by magnetic clouds and ICME sheath regions. Geophysical research letters, 34(2) , 2007.

Reeves G. D., K. L. McAdams, R. H. W. Friedel, and T. P. O'Brien. Acceleration and loss of relativistic electrons during geomagnetic storms, Geophys. Res. Lett., 30(10), 1529, 2003. doi:10.1029/2002GL016513.

Regnault F., Janvier M., Démoulin P., Auchère F., Strugarek A., Dasso S., &Noûs C., 20 years of ace data: How superposed epoch analyses reveal generic features in interplanetary CME profiles. Journal of Geophysical Research: Space Physics, 125, e2020JA028150,2020 https://doi.org/10. 1029/2020JA028150

Revah I., & Bauer P. , Rapport d'activité CRPE pourl'année1981. CentredeRecherchesEnPhysique de l'Environnement Terrestre Et Planétaire, Note technique CRPE(115), 1983

Scurry L., and C. T. Russell. Proxy studies of energy transfer to the magnetopause, J. Geophys. Res., 96, 9541, 1991

Stamper R., M. Lockwood, M. N. Wild, and T. D. G. Clark (1999), Solar causes of the long-term increase in geomagnetic activity, J. Geophys. Res., 104(A12), 28,325–28,342, 1999. doi:10.1029/1999JA900311.

Taylor J. R., Lester M., and Yeoman T. K.: A superposed epoch analysis of geomagnetic storms, Ann. Geophys., 12, 612–624, 1994 https://doi.org/10.1007/s00585-994-0612-4

Temerin M., and X. Li, Dst model for 1995– 2002, J. Geophys. Res., 111, A04221, 2006. doi:10.1029/2005JA011257.

Tsurutani Bruce T. , Walter D. Gonzalez. The cause of high-intensity long-duration continuous AE activity (HILDCAAs): Interplanetary Alfvén wave trains, Planetary and Space Science Vol. 35, Issue 4, pp. 405-412, 1987

Vasyliunas V. M., J. R. Kan, G. L. Siscoe, and S. I. Akasofu. Scaling relations governing magnetospheric energy-transfer, Planet. Space Sci., 30(4), 359–365, 1982. doi:10.1016/0032-0633(82)90041-1.

Vichare G., S. Alex, and G. S. Lakhina, Some characteristics of intense geomagnetic storms and their energy budget, J. Geophys. Res., 110, A03204, 2005. doi:10.1029/2004JA010418

Walach M.-T., & Grocott A. SuperDARN observations during geomagnetic storms, geomagnetically active times, and enhanced solar wind driving. Journal of Geophysical Research: Space Physics, 124, 5828–5847, 2019 https://doi.org/10.1029/ 2019JA026816 ,

Walton S. D. and Kyle R. Murphy. Superposed epoch analysis using time-normalization: A Python tool for statistical event analysis. Frontiers in Astronomy and Space Sciences, 2022. doi: 10.3389/fspas.2022.1000145

Wang C., J. P. Han, H. Li, Z. Peng,and J. D. Richardson, Solarwind-magnetosphere energy cou-pling function fitting: Results from a global MHD simulation, J. Geophys.Res. Space Physics, 119, 6199–6212, 2014 doi:10.1002/2014JA019834.

Wu C., Liou K., Lepping R. P., Hutting L., Plunkett S., Howard R. A., & Socker D., The first super geomagnetic storm of solar cycle 24: "The St. Patrick's Day event (17 March 2015)". Earth, Planets and Space, 68(1), 151, 2016.

Wu L., Gendrin R., Higel B., & Berchem J. Relationships between the solar wind electric field and the magnetospheric convection electric field. geophysical research letters, 8(10), 1090–1102, 1981

Wygant J. R., R. B. Torbert, and F. S. Mozer. Comparison of S3-3 polar cap potential drops with the interplanetary magnetic field and mod els of magnetopause reconnection, J. Geophys. Res., 88, 5727, 1983

Xu W.-y., and E.-Q. Shi , Numerical examination of Akasofu's energy coupling function, Chin. J. Space Sci., 6(1), 24–3232, 1986

Yermolaev Y. I., Nikolaeva N. S., Lodkina I. G., & Yermolaev M. Y. Specific interplanetary conditions for CIR-Sheath-and ICME-induced geomagnetic storms obtained by double superposed epoch analysis. Annales Geophysicae, 28(12), 2177–2186, 2010. https://doi.org/10.5194/angeo-28-2177-2010

Yokoyama N., & Kamide Y. Statistical nature of geomagnetic storms. Journal of GeophysicalResearch, 102(A7), 14215–14222, 1997. https://doi.org/10.1029/97JA00903